Neurovascular Uncoupling: Multimodal Imaging Delineates the Acute Effects of MDMA

Tudor M. Ionescu [1], Mario Amend [1], Tadashi Watabe [1,2], Jun Hatazawa [2], Andreas Maurer[1], Gerald Reischl[1,3], Bernd J. Pichler [1,3], Hans F. Wehrl [1]*, Kristina Herfert [1]*

* contributed equally

[1] Werner Siemens Imaging Center, Department of Preclinical Imaging and Radiopharmacy, Eberhard Karls University Tuebingen, Germany

[2] Department of Nuclear Medicine and Tracer Kinetics, Osaka University, Japan

[3.]Cluster of Excellence iFIT (EXC 2180) "Image Guided and Functionally Instructed Tumor Therapies", University of Tübingen, Germany

Corresponding author: Prof. Dr. Kristina Herfert (kristina.herfert@med.uni-tuebingen.de)

Address: Roentgenweg 13, 72076 Tuebingen, Germany, Tel: +49 7071 29 87680

Abstract

Psychedelic compounds have attracted increasing interest in recent years due to their therapeutic potential for psychiatric disorders. Methylenedioxymethamphetamine (MDMA) is currently being investigated in clinical trials to treat post-traumatic stress disorder. To understand the acute effects of psychedelic drugs *in vivo*, functional MR imaging (fMRI) has been widely used in recent years. Notably, fMRI studies have shown that MDMA leads to inhibition of brain activity, challenging earlier hypotheses indicating mainly excitatory effects. However, interpretation of hemodynamic changes induced by psychedelics is challenging because of the potent vascular effects associated with this class of substances. Therefore, this study aimed to investigate the acute effects of MDMA using simultaneous positron emission tomography (PET)/fMRI in rats. For this purpose, hemodynamic changes measured by BOLD-fMRI were related to alterations in glucose utilization and serotonin transporter (SERT) occupancy, investigated using [^{18}F]FDG functional PET (fPET) and [^{11}C]DASB PET.

We demonstrate that MDMA induces global hemodynamic decreases accompanied by localized metabolic increases. Elevated metabolism was found primarily in limbic projection areas involved in emotion processing. Concurrent BOLD-fMRI decreases, also found in extracerebral areas, indicate that the BOLD-fMRI reductions observed in the brain are of vascular, non-neuronal origin. We further show that higher SERT occupancy strongly correlates with regional BOLD-fMRI reductions. Therefore, increased serotonin levels induced by SERT blockage may cause a neurovascular uncoupling.

Correct understanding of the *in vivo* mechanism of MDMA not only supports ongoing research but also warrants a reassessment of previous studies on neuronal effects of psychedelics relying on neurovascular coupling.

1. Introduction

In recent years psychedelic drugs, including lysergic acid diethylamide (LSD), psilocybin, and methylenedioxymethamphetamine (MDMA), have gained increasing attention due to their potential medical benefit for the treatment of psychiatric disorders [1, 2]. MDMA-assisted psychotherapy is currently in a phase three clinical trial to treat severe post-traumatic stress disorder (PTSD) with encouraging initial results [3]. Research in this area is also increasingly associated with the development

of imaging techniques as quantitative biomarkers in addition to behavioral parameters [1]. To investigate the mechanisms of psychedelic drugs *in vivo*, magnetic resonance imaging (MRI) methods inferring neuronal activity through neurovascular coupling, such as blood oxygenation level-dependent functional MRI (BOLD-fMRI) and arterial spin labeling (ASL), have been widely used [4-8]. Interestingly, research performed over the last decade using the aforementioned methods has shown that psychedelic compounds such as MDMA [4] and psilocybin [6] inhibit brain activity, contradicting previous studies that indicated mainly excitatory effects [9-12].

However, the use of hemodynamic methods may be insufficient to understand the effects of psychedelics on neuronal activity. First, psychedelic drugs elicit their effects by strongly affecting one or more neurotransmitter systems [13]. Thus, it is crucial to evaluate hemodynamic changes in the context of changes in the respective neurotransmitter systems. Second, in addition to neuronal effects, increased neurotransmitter concentrations such as serotonin and dopamine elicited by psychedelic compounds can have potent vascular effects [14-16]. This aspect is particularly critical for methods based on neurovascular coupling, such as BOLD-fMRI and ASL. The emergence of hybrid positron emission tomography (PET)/MRI allows simultaneous assessment of brain function at multiple physiological levels [17, 18]. The combination of PET and pharmacological MRI (phMRI) [19] can provide high complementary measures of the effect of pharmacological compounds, especially for the evaluation of drug effects [20, 21]. In addition, recent developments in the administration of 2-[^{18}F]fluoro-2-deoxyglucose ([^{18}F]FDG) PET protocols via constant infusion [22] have paved the way towards functional PET (fPET) [22], a technique that allows imaging of changes in glucose metabolism at a temporal resolution of minutes [23]. fPET overcomes the lack of temporal resolution in previous studies, allows imaging of effects within a scan and provides a more robust indirect measure of neuronal activity compared to fMRI, because it is independent of changes in hemodynamics [22].

Here, we aimed to characterize the acute effects of MDMA using simultaneous PET/fMRI. First, we performed [^{18}F]FDG fPET/fMRI scans to simultaneously determine hemodynamic and metabolic changes elicited by MDMA. In a second cohort, because the serotonin transporter (SERT) is one of the main targets of

MDMA [24], we used the SERT PET ligand [^{11}C]-3-amino-4-(2-dimethylaminomethylphenylsulfanyl)-benzonitrile ([^{11}C]DASB) [25] to investigate whether SERT blockage by MDMA correlates with changes in BOLD-fMRI across the brain. The overall goal of this study was to exploit the potential of multimodal imaging for complementary detection and characterization of the acute *in vivo* effects of MDMA. By simultaneously acquiring data on hemodynamics, metabolism, and SERT occupancy, we aimed to test the two conflicting hypotheses that MDMA has either mainly inhibitory or excitatory effects on brain activity. A detailed description of the effects of MDMA will help to understand the mechanisms of the drug in the treatment of psychiatric disorders such as PTSD through MDMA-assisted psychotherapy, performed under acute MDMA.

2. Material and Methods

Animals

Male Lewis rats (n = 29) were obtained from Charles River Laboratories (Sulzfeld, Germany) and divided into two groups: [^{18}F]FDG fPET/fMRI scans were performed in 17 animals (361 ± 19 g), while [^{11}C]DASB PET/fMRI were performed in 11 animals (365 ± 19 g). Nine fMRI datasets were excluded from the study due to motion during acquisition. One [^{11}C]DASB PET and two [^{18}F]FDG fPET datasets were excluded from the analysis because of paravenous tracer injections. The animals were kept at a room temperature of 22 °C and 40-60% humidity under a 12-hour light-dark cycle. The rats were fed with standard diet and received tap water *ad libitum.* Animals were fasted for six hours before the start of the experiments. All experiments were performed in accordance with the German Federal Regulations on the Use and Care of Laboratory Animals and approved by the Tübingen regional council.

Two additional sets of subjects scanned under the same [^{18}F]FDG fPET/fMRI and [^{11}C]DASB PET/fMRI protocols, but exposed to PBS instead of MDMA, are presented in the *supplementary information.*

Simultaneous PET/fMRI experiments

Animals were placed in knock-out boxes, and anesthesia was induced with 3% isoflurane in regular air. Reflex tests were performed to determine sufficient sedation.

For subsequent preparation procedures, the isoflurane concentration was reduced to 2%. After the weight of the animals was determined, a catheter with a 30-G needle was positioned in a tail vein to administer the radioactive tracer. Another catheter was placed into the other tail vein for MDMA administration. Animals were then placed on a dedicated temperature-controlled small animal bed (Medres, Cologne, Germany). The temperature was monitored and maintained at 36.5°C with a rectal probe, and respiratory rates were monitored using a breathing pad. Rats were then placed in the scanner, and the isoflurane concentration was decreased to 1.3% throughout the scan.

Scans were performed using a 7-T small-animal MRI scanner (ClinScan, Bruker Biospin, Ettlingen, Germany) using a 72-mm-diameter linearly polarized RF coil (Bruker) for transmission and a four-channel rat brain coil (Bruker) for reception. First, localizer scans were performed to position the brains in the center of the field of view. Local magnetic field maps were then generated to optimize local field homogeneity. Subsequently, T2-weighted MRI sequences (TR: 1800 ms, TE: 67.11 ms, FOV: 40 x 32 x 32 mm^3, image size: 160 x 128 x 128 px, Rare factor: 28, averages: 1) were performed to obtain anatomical references. Finally, fMRI imaging was performed using T2*-weighted gradient-echo EPI sequences (TR: 2000ms, TE: 18ms, 0.25 mm isotropic resolution, FoV 25 x 23 mm^2, image size: 92 x 85 x 20 px, slice thickness: 0.8 mm, 20 slices).

Simultaneously, PET scans were acquired using a PET insert developed in collaboration with Bruker, which is the second generation of an insert previously developed in-house [18]. Protocols for tracer synthesis, injected radioactivities and molar activities are given in *supplementary information.* PET and fMRI acquisitions were started simultaneously 30 seconds before tracer injection and performed over 100 minutes after tracer injection. PET data were saved as list-mode files for later reconstruction into dynamic scans of 100 1-minute frames using an ordered-subsets expectation maximization 2D (OSEM-2D) algorithm.

A pharmacological MDMA challenge of 3.2 mg/kg was administered 40 minutes after tracer injection over 30 seconds.

Data preprocessing

Statistical Parametric Mapping 12 (SPM 12, Wellcome Trust Centre for Neuroimaging, University College London, London, United Kingdom) via Matlab (The MathWorks, Natick, MA, USA) and Analysis of Functional NeuroImages (AFNI, National Institute of Mental Health (NIMH), Bethesda, Maryland, USA) were used for data preprocessing as previously reported [26]. An extensive description of all preprocessing steps performed can be found in the *supplementary information.*

To analyze the effect of non-neuronal signal changes on the brain BOLD-fMRI measures, we extracted the average signal from all voxels in areas outside the brain using masks created in AFNI. Average time courses were extracted from all datasets after preprocessing using the MarsBaR toolbox [27] and regions of interest defined by the Schiffer brain atlas [28]. For a complete list of the regions, please refer to *supplementary information*.

SPM data analysis

The general linear model (GLM) available in SPM was applied to determine voxels with significantly altered fMRI and PET signals after MDMA exposure. For all datasets, the baseline was defined as the period between 30 and 40 minutes after scan start, after tracer equilibrium had been reached between the high target and the reference regions. The [^{18}F]FDG fPET data were normalized based on cerebellar uptake, as previously recommended [29], whereas for [^{11}C]DASB PET, the cerebellar gray matter was chosen as the reference region [30].

For PET data analysis, mean images of the dynamic 1-minute frames were generated over seven measurement periods: between 30 and 40 minutes following tracer injection as baseline, and for each of the subsequent 10-minute periods after MDMA exposure (40-50 minutes, 50-60 minutes, 60-70 minutes, 70-80 minutes, 80-90 minutes and 90-100 minutes after scan start). Paired t-maps were then calculated between the baseline and each block after MDMA for [^{18}F]FDG using voxel-wise normalized uptake maps and for [^{11}C]DASB using voxel-wise DVR-1 maps. For more details please refer to *supplementary information.*

For fMRI, a first-level analysis was applied to the individual scans using the pseudo-block approach reported for phMRI [31, 32]. To allow a direct comparison with the

PET readout, the same six 10-minute blocks between MDMA challenge and the end of the scans (40-50 minutes, 50-60 minutes, 60-70 minutes, 70-80 minutes, 80-90 minutes, and 90-100 minutes after scan start) were compared with the baseline 10-minute block before MDMA injection. After estimating the GLM parameters, statistical parametric maps were generated by interrogating the data using contrast vectors between each block after MDMA and baseline. The generated maps were then used to delineate group-level effects through a second-level analysis. Initially, binary masks were used to perform the analyses only within the brain. The binary masks were removed for later analysis of extracerebral hemodynamic alterations.

All group-level t-maps were subjected to voxel-wise signal quantification to determine the regional contributions of brain regions selected according to the Schiffer brain atlas [28]. The average t-scores of all voxels comprising each region were calculated for each period and modality to compare the respective spatial patterns of MDMA effects on hemodynamics, glucose metabolism, and SERT occupancy.

3. Results

Metabolic increases accompany hemodynamic reductions after MDMA

First, we investigated the relationship between acute hemodynamic and metabolic changes following acute MDMA using a simultaneous [^{18}F]FDG fPET/fMRI protocol (Figure 1).

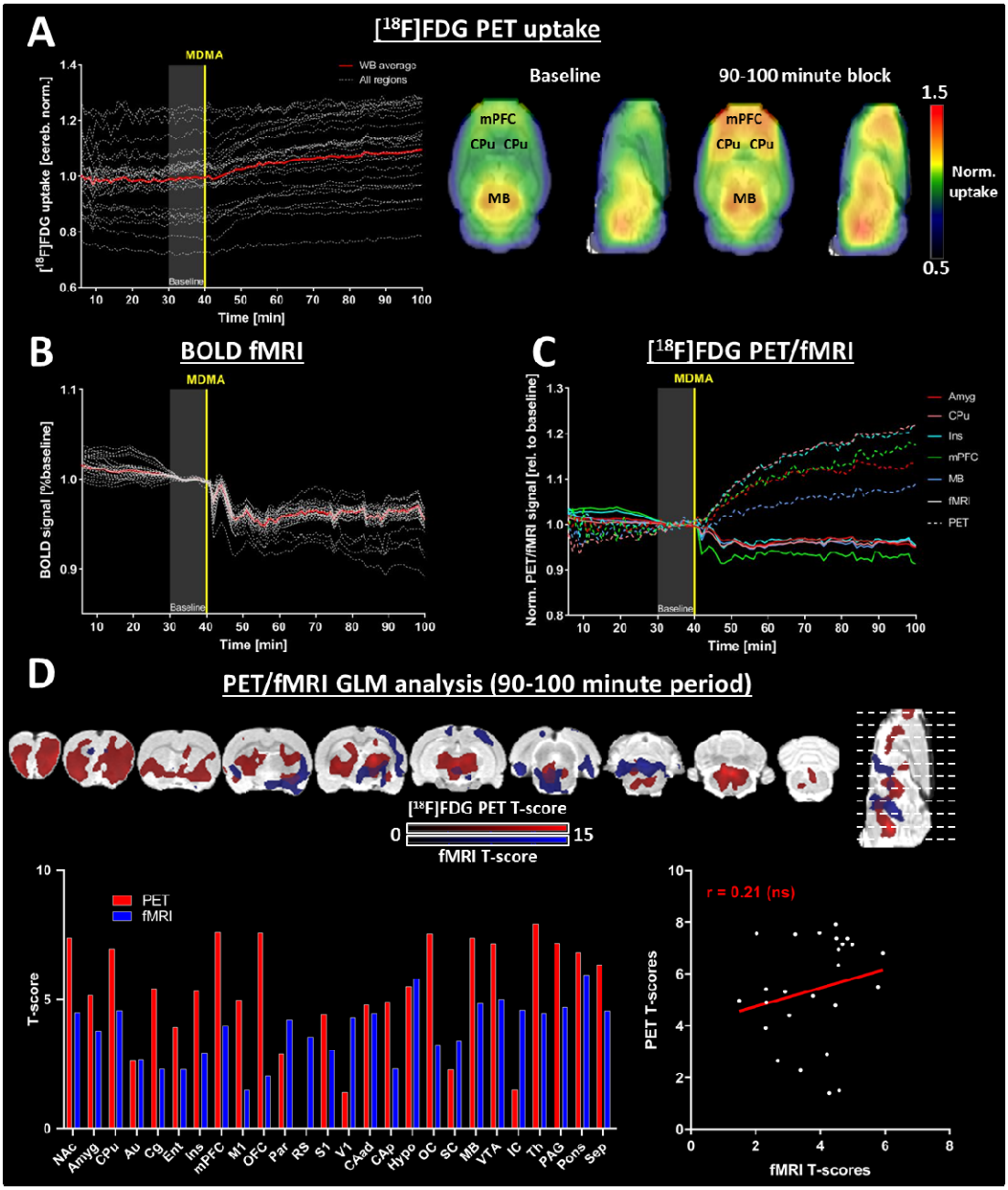

Figure 1: Region-wise and voxel-wise evaluation of [^{18}F]FDG fPET and BOLD-fMRI signals changes. (A) TACs for all regions and whole-brain average. Voxel-wise normalized uptake maps

indicate [^{18}F]FDG uptake at baseline (30 to 40 minutes after scan start), as well as 50-60 minutes after MDMA administration. (B) Regional BOLD-fMRI signals normalized to respective baselines (average regional BOLD-fMRI signals in the period 30-40 minutes after scan start). (C) Both signals were normalized to the baseline period over the last ten minutes before MDMA administration for a common frame of reference. Continuous lines indicate the BOLD-fMRI signals, interrupted lines the [^{18}F]FDG fPET signals in Amyg, CPu, Ins, mPFC, and MB. (D) Voxel-wise analysis of both signals in the period 50-60 minutes after MDMA challenge. The voxelwise maps are presented at $p < 0.05$ (FWE-corrected at voxel level) for PET and $p < 0.001$ at voxel level with $p < 0.05$ FWE correction at cluster level for fMRI ($n = 15$ for fPET, $n = 9$ for fMRI). The bar diagram indicates average t-scores for each region and both modalities. The average regional t-scores are plotted in a scatter diagram to evaluate the spatial correlation of both readouts. Abbreviations: GLM = general linear model, ns = not significant. For abbreviations of the different regions, please refer to *Supplementary Information*.

The normalized [^{18}F]FDG fPET TACs of all regions and the average whole-brain TAC are shown in Figure 1A. Visual assessment of TACs and voxel-wise uptake maps indicated an increase in metabolism in the midbrain and subcortical areas such as the striatum and frontal cortical areas, whereas more minor or no changes occurred in posterior cortical regions. Notably, we found a simultaneous decrease in hemodynamics, as indicated by BOLD-fMRI (Figure 1B). The whole-brain averaged BOLD-fMRI signal was reduced by 4.5% fifteen minutes after the challenge. Importantly, the data revealed that the decreases were of global nature and occurred in all regions investigated.

A temporal comparison of the [^{18}F]FDG fPET and BOLD signal changes relative to baseline is shown in Figure 1C. The highest metabolic increases occurred in frontal areas, including the CPu (22% increase 60 minutes post-challenge), Ins (21% increase 60 minutes post-challenge), mPFC (18% increase 58 minutes post-challenge), and Amyg (13.5% increase 58 minutes post-challenge). Temporally, increases in all regions (>1%) were observed within 5 minutes of challenge.

The voxel-wise GLM analyses presented in Figure 1D revealed that the metabolic rate increased across several subcortical areas and in frontal cortical areas in the period between 50 and 60 minutes after the challenge. The mPFC and OFC ($t = 7.6$ for both), along with MB ($t = 7.4$), Th ($t = 7.9$) and NAc ($t = 7.4$) exhibited the most significant [^{18}F]FDG increases. The most significant BOLD-fMRI decreases occurred in posterior areas such as the MB ($t = 4.8$), VTA ($t = 5.0$), Hypo ($t = 5.8$), and Pons ($t = 5.9$). The t-scores of metabolic increases and BOLD-fMRI decreases did not

238 correlate significantly (r = 0.21), underlining a disturbed relationship between
239 metabolism and hemodynamics.

240 **SERT occupancy changes induced by MDMA correlate with BOLD decreases**

241 To further elucidate the molecular underpinnings of the observed hemodynamic
242 decreases, we evaluated BOLD-fMRI changes concurrently with alterations in SERT
243 availability using [^{11}C]DASB PET/fMRI in a second cohort (Figure 2).

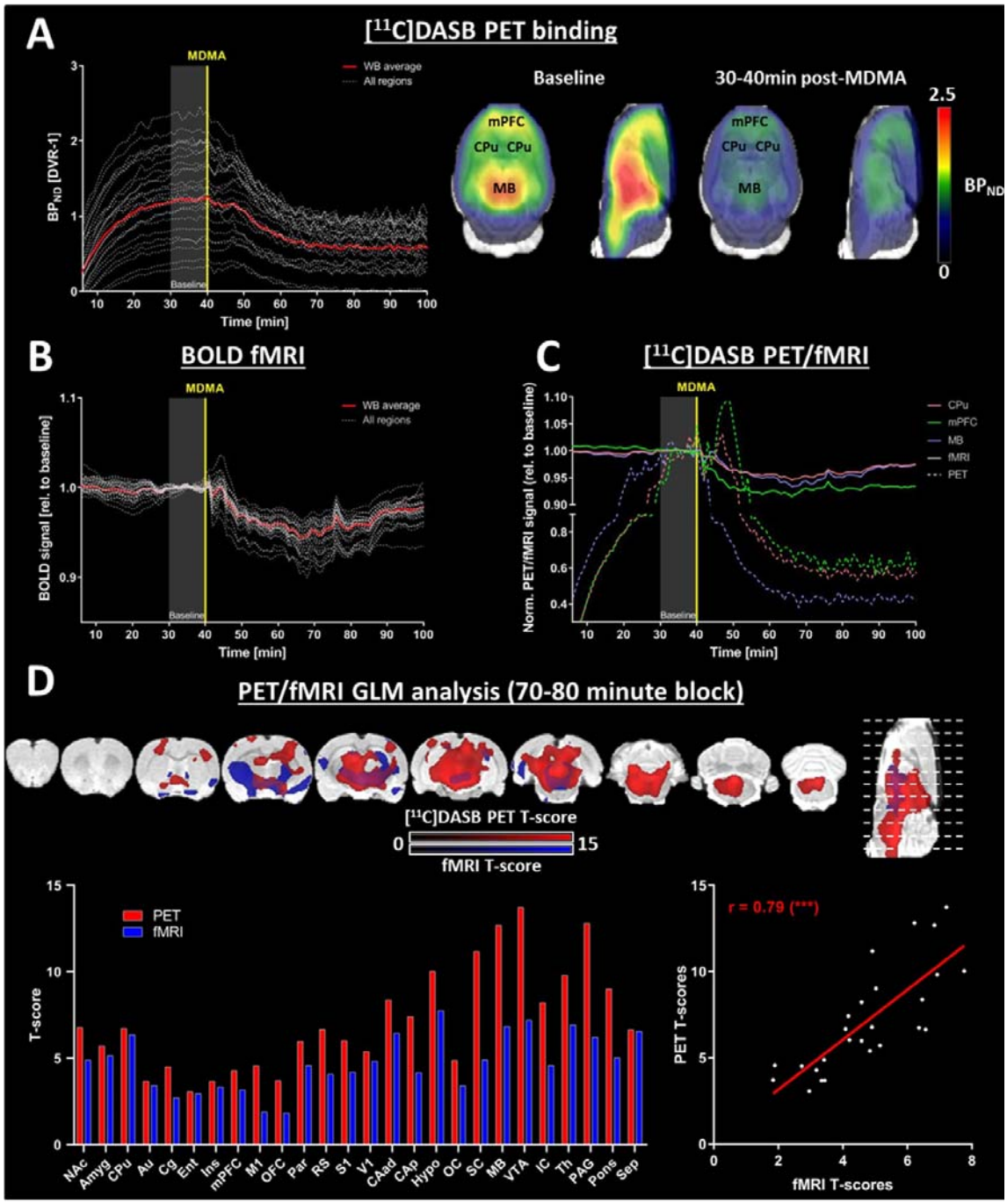

Figure 2: Region-wise and voxel-wise evaluation of [^{11}C]DASB PET and BOLD-fMRI signal changes (A) Dynamic binding potentials for all regions and whole-brain average. Voxel-wise binding potential maps indicate [^{11}C]DASB binding at baseline (30 to 40 minutes after scan start), as well as 70-80 minutes after scan start (30-40 minutes post-challenge). **(B)** Regional BOLD-fMRI signals normalized to respective baselines (average regional BOLD-fMRI signal in the period 30-40 minutes after scan start). **(C)** Temporal comparison of PET and BOLD signal changes (normalized to the baseline) in CPu, mPFC, and MB. **(D)** Voxel-wise analysis of both signals in the period 30-40 minutes

after MDMA challenge. The voxelwise maps are presented at $p < 0.05$ (FWE-corrected at voxel level) for PET and $p < 0.001$ at voxel level with $p < 0.05$ FWE correction at cluster level for fMRI ($n = 11$). The bar diagram indicates average t-scores for each region and both modalities. The average regional t-scores are plotted in a scatter diagram to evaluate spatial correlation of both readouts (*** indicates significance at $p < 0.001$). Abbreviation: GLM = general linear model; for abbreviations of the different regions please refer to *Supplementary Information*.

The DVR-1 of [^{11}C]DASB reached equilibrium 30 minutes after injection (Figure 2A). After pharmacological challenge with MDMA, binding values in all regions decreased either immediately (1-2 minutes after the challenge) in areas with high binding values ($BP_{ND} > 1.8$) or with a delay after approximately 10 minutes in regions with lower [^{11}C]DASB binding values. At 30 minutes post-challenge, the binding values remained stable until the end of the scan period. Voxel-wise binding values reflected the most significant decreases of [^{11}C]DASB binding in regions with high SERT availability. Similarly to the BOLD-fMRI dataset acquired in the [^{18}F]FDG fPET/fMRI cohort, all regional BOLD signals decreased within 6 minutes of MDMA challenge (Figure 2B). Fifteen minutes after the MDMA challenge, the whole-brain average BOLD signal was decreased by 4% compared to baseline.

A temporal comparison of the changes in [^{11}C]DASB binding and the BOLD-fMRI responses for three exemplary regions (Figure 2C) revealed that regions with higher baseline SERT availability showed a faster response than regions with lower baseline SERT availability. For example, [^{11}C]DASB binding in the MB, a region with high baseline [^{11}C]DASB binding ($BP_{ND} = 2.1$), decreased one minute after challenge reaching 59% of its baseline value at 40 minutes after the challenge. In contrast, [^{11}C]DASB binding in the CPu ($BP_{ND} = 1.6$) and mPFC ($BP_{ND} = 1.6$) remained stable or increased shortly after the MDMA challenge. After approximately 10 minutes, [^{11}C]DASB binding decreased in all regions until it reached equilibrium at 30-40 minutes after the challenge (39% decrease for mPFC, 44% decrease for CPu 40 minutes post-challenge compared to baseline). Compared to the temporally differentiated [^{11}C]DASB binding reductions delineated above, decreases in BOLD occurred homogeneously. The highest regional BOLD decreases occurred within the first 30 minutes after challenge. Reductions between 1% and 2% could be observed for mPFC, CPu, and MB as early as 2 minutes after challenge. The decreases peaked within 30 minutes after MDMA injection (~8.5% in mPFC, ~5.5% in CPu, and ~6.5% in MB).

Figure 2D shows GLM analyses for both readouts between baseline and 70-80 minutes after the start of the scan, when changes reached a plateau for both methods. [^{11}C]DASB decreases were highest in the VTA (t = 13.7), PAG (t = 12.8) and MB (t = 12.7), regions with high baseline [^{11}C]DASB binding values. The largest regional t-scores for BOLD-fMRI occurred in the Hypo (t = 7.8), VTA (t = 7.2) and Th (t = 6.9). Remarkably, regional t-scores of both readouts correlated strongly ($r = 0.79$, $p < 0.001$), indicating a strong relationship between SERT occupancy and BOLD signal decreases.

Hemodynamic reductions also occur in non-neuronal tissues

The smaller spatial extent of hemodynamic changes compared with the metabolic and SERT occupancy changes presented for the two cohorts above may be due to the smaller magnitudes of the BOLD decreases. To further clarify this aspect, we merged the fMRI scans from both cohorts (Figure 3). We also extracted the BOLD signals from extracerebral areas to investigate whether the BOLD decreases are specific to neuronal tissue. Finally, we compared the temporal characteristics of hemodynamic, metabolic, and SERT occupancy changes.

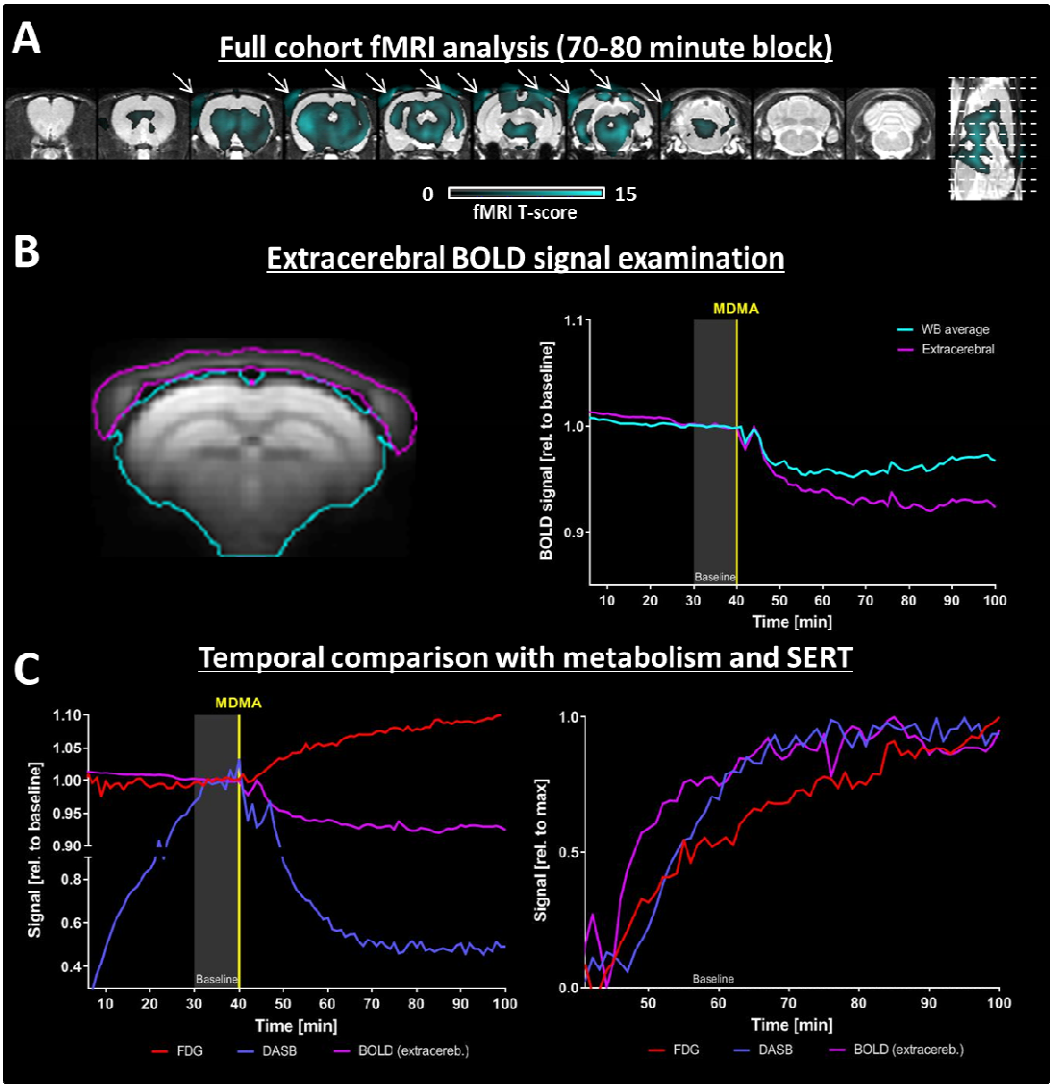

Figure 3: Examination of BOLD signal changes in extracerebral areas. (A) GLM analysis of BOLD decreases after merging BOLD-fMRI datasets acquired in both [^{18}F]FDG and [^{11}C]DASB cohorts (n=20). Data are shown at $p < 0.05$, FWE-corrected at the voxel level. Arrows indicate extracerebral decreases. **(B)** BOLD signals were extracted from the extracerebellar regions (indicated in cyan), averaged over the cohort, and plotted along with the group-average whole-brain signal. **(C)** Left: Temporal alterations of the three signals in relation to the baseline. Right: Temporal changes of the readouts after MDMA challenge relative to their respective maximum changes (0 = no change, 1 = maximum change) are shown in order to depict the temporal evolution of the alterations.

Because of the global nature of the observed hemodynamic decreases, we also investigated changes in BOLD signal without masking extracerebral areas (Figure 3A). The analysis indicates the decrease in BOLD-fMRI is widespread and comparable in magnitude to the decrease in [^{11}C]DASB PET binding and, intriguingly, also occurs in non-neuronal areas. Thus, we extracted BOLD signals from

extracerebral areas consisting predominantly of tissue surrounding the skull (Figure 3B) to determine the temporal characteristics of the observed decreases. Remarkably, the extracerebral BOLD signal decreased coherently with the cerebral BOLD signal, both reaching maximum reductions 27 minutes after the challenge (4.8% for cerebral BOLD signal and 7.4% for extracerebral BOLD signal).

The temporal profiles of the changes in hemodynamics, metabolism, and SERT occupancy are shown in **Error! Reference source not found.**C and D, respectively. The temporal characteristics of hemodynamic and SERT availability decreases were highly comparable, both reaching 90% of their maximum changes 30 minutes after the challenge. In contrast to the other two datasets, [^{18}F]FDG increased linearly, reaching 90% of the maximum change only 45 minutes after the challenge, with the whole-brain average [^{18}F]FDG TAC continuing to increase until the end of the scan. This finding suggests that metabolic increase may persist longer than one hour after the MDMA challenge included in the scans.

4. Discussion

In this study, we investigated the acute effects of the psychedelic drug MDMA using simultaneous PET/fMRI. For this purpose, we examined the relationships between changes in glucose metabolism, vascular responses, and SERT availability in different brain regions. We detected concurrent localized increases in glucose consumption and hemodynamic decreases of global nature, both occurring within minutes after MDMA exposure. Furthermore, as expected, we identified decreased [^{11}C]DASB specific binding to the SERT following the challenge. Remarkably, regional SERT changes correlated strongly with decreased hemodynamics, whereas increased glucose metabolism measured by [^{18}F]FDG fPET showed no correlation with BOLD reductions. Finally, we show that hemodynamic decreases concurrently take place in non-neuronal extracerebral tissues. Our data suggest that increased neuronal activity is accompanied by neurovascular uncoupling, possibly mediated through the vascular effects of serotonin following SERT blockage.

Simultaneous uncoupling between metabolism and hemodynamics

The acute *in vivo* effects of psychedelic compounds, and MDMA in particular, have not been fully elucidated in terms of neuronal activation or inhibition, with two

hypotheses being postulated. *In vivo*, studies measuring glucose utilization have shown mixed results, yet mainly increased metabolism following psychedelic challenges [9, 10, 12, 33], suggesting neuronal activation. However, more recent work with ASL challenged this hypothesis and argued that brain activity is decreased under MDMA [4]. Interestingly, the authors did not find any hemodynamic increase following MDMA across the entire brain. Our study confirms that this finding also holds when applying an acute MDMA challenge in rodents. Furthermore, the authors speculated that MDMA exerts inhibitory effects directly through 5-HT_{1A} receptors, which are known to induce hyperpolarization and decrease firing rates [4, 34]. The same group found similar hemodynamic decreases under acute psilocybin [6], postulated by the authors to be driven by inhibitory effects of 5-HT_{2A} receptors [35]. On a side note, the decreases in ASL and BOLD previously observed for MDMA and psilocybin in humans were also asymmetric [4, 36], with a focus on the right cerebral hemisphere. The same pattern can be observed in our study, supporting the translatability of our readout. Notably, the authors argued that possible discrepancies with previous work indicating increased metabolism using [^{18}F]FDG PET [12] might be because [^{18}F]FDG PET operates on a much longer time scale than fMRI [6]. Therefore, the authors claimed that the increases in earlier [^{18}F]FDG PET studies may represent a rebound in glucose metabolism after the actual acute inhibitory effects captured by fMRI [6]. We agree with the above statement that earlier [^{18}F]FDG PET or *ex vivo* studies [9, 10, 12, 33] measuring cerebral glucose utilization lacked temporal specificity because of the paradigms used, which complicates the interpretation of results for acute effects. Earlier work on blood flow effects is similarly inconclusive and partly confirmes the general decreases induced by MDMA seen with ASL [4, 9]; however, CBF measurements using [^{15}O]H_2O PET indicated mixed regional increases and decreases [37]. A further reason for the partially conflicting results of the above studies is that the conclusions were drawn between different, relatively small cohorts having received either placebo or MDMA.

In our study, the above limitations of previous studies were overcome. Recently developed PET protocols have enabled the detection of metabolic effects at high temporal resolutions of only a few minutes [22, 23]. Our similarly designed study allowed temporal assessment of the acute effects of two pairs of readouts: metabolic versus hemodynamic response and SERT occupancy versus hemodynamics. The effects were delineated (1) immediately after the challenge at 1-minute intervals, (2)

simultaneously for both pairs of measurements, and (3) in the same animals, thus avoiding the comparison of two different groups of subjects. Therefore, we demonstrate that the uncoupling between flow and metabolism suggested in previous work [9, 14, 33] does occur in the same subjects and almost simultaneously.

Origin of peripheral and cerebral hemodynamic effects

We show that non-neuronal effects dominate hemodynamic changes induced by MDMA. In particular, our data shed light on two separate phenomena. First, temporal coherence between hemodynamic reductions in cerebral and extracerebral areas suggests that vascular effects occur in the periphery. The 5-HT_{2A}, which is postulated, along with the 5-HT_{1B} receptor, to mediate vasoconstrictive effects [38, 39], is one of the main targets of MDMA [5, 36]. However, because MDMA has a much stronger affinity to the 5-HT_{2A} receptor than to the 5-HT_{1B} receptor [5], direct agonist action of MDMA at the 5-HT_{2A} in peripheral blood vessels likely results in vasoconstriction [38]. This is supported by work showing that the use of 5-HT_{2A} antagonists following the elevation of serotonin levels reduces the serotonin-induced vasoconstriction in the carotid artery, the main vessel that provides blood supply to the brain [40]. Furthermore, compounds with high selectivity for 5-HT_{2A} have been shown to increase blood pressure in carotid arteries, indicating vasoconstrictive effects [41].

In addition to the peripheral effects of MDMA, the reductions observed in the brain are likely also of direct serotonergic nature, consistent with the previously reported effects of serotonin on brain microvasculature [15, 16]. Early work has shown that manipulation of the raphé nuclei directly affects brain microcirculation by inducing vasoconstriction [14]. Interestingly, although both MDMA and psilocybin act potently on the serotonergic system, psilocybin has a very low affinity to the SERT, unlike MDMA [42, 43]. Based on this fact, it is interesting that both drugs appear to induce similar spatial patterns of hemodynamic decreases [4, 6]. Since of all serotonergic receptors, psilocybin has the highest affinity to the 5-HT_{2A} receptor [43], which has been shown to induce vasoconstriction peripherally, it is reasonable to assume that this is similar in the brain. In contrast to the peripheral effects of MDMA, which can be attributed solely to the direct effects of the drug, the observed decreases in the brain may additionally be triggered by increased synaptic serotonin levels following SERT blockage. This finding is supported by the very high correlation between SERT

414 blockage and hemodynamic decreases in BOLD-fMRI, suggesting that direct effect of
415 endogenous serotonin may additionally modulate hemodynamic decreases in the
416 brain. In the future, further insight may be gained by combining a psychedelic
417 challenge with antagonists to 5-HT_{2A} and other serotonin receptors to elucidate their
418 respective involvements in the observed hemodynamic decreases.

419 Our results warrant a re-evaluation of the hypothesis that the observed hemodynamic
420 reductions by psychedelic drugs are driven by neuronal activity, which is also
421 supported and discussed in later publications [44-47]. In general, additional caution is
422 necessary when interpreting findings relying on neurovascular coupling, such as
423 BOLD-fMRI functional connectivity studies, under pharmacological challenges [4, 5,
424 36].

425 **Spatial and temporal properties of increased metabolism**

426 We demonstrate that MDMA triggers increased glucose consumption, likely due to
427 neuronal activation, in different regions by [^{18}F]FDG fPET measurements. Changes
428 in [^{18}F]FDG fPET have been shown to reliably reflect changes in neuronal activity
429 while being independent of hemodynamic changes [22]. Our data revealed a
430 substantial increase in metabolic activity that started a few minutes after MDMA
431 injection and extended from the raphé nuclei to anterior subcortical and cortical
432 projection areas. Interestingly, although many increases in glucose consumption
433 overlapped with SERT blockage, the metabolic increases were more weighted
434 toward projection areas than the reductions seen in [^{11}C]DASB binding. First, this
435 finding is in line with the hypothesis that the majority of glucose is consumed
436 postsynaptically [48, 49]. Second, the areas showing increased metabolism are
437 consistent at a functional level with the majority of previously reported behavioral
438 effects of MDMA. The signals observed in the nucleus accumbens, amygdala, and
439 insula compare well with salience changes known from imaging and behavioral
440 studies [4, 50]. In particular, the nucleus accumbens, as the main reward processing
441 hub, is involved in responses to numerous drugs [51]. In addition, the amygdala,
442 insula, and orbitofrontal cortex are strongly involved in emotional processes [52], so
443 their increased activities could explain the enhanced emotionality and empathy
444 reported as effects of the drug [53]. Activity in the olfactory cortex and olfactory bulb
445 could indicate increased food-seeking or sexual arousal [53, 54]. Enhanced
446 metabolic activity in sensory cortices is in concordance with heightened sensations

elicited by MDMA [53]. At the molecular level, the aforementioned 5-HT_{2A} receptor exhibits a strong anterior-posterior gradient in the cortex, with strong expression in frontal areas and less expression in posterior areas of the cortex [55], consistent with the activations indicated by our [^{18}F]FDG PET data, predominantly in frontal cortical areas. Moreover, the 5-HT_{2A} receptor has been shown to be responsible for serotonergic activation in projection areas such as the prefrontal cortex [56, 57]. However, the exact receptors involved in neuronal activation indicated by fPET can only be speculated because both MDMA and endogenous serotonin may play a role, both of which can bind to a wide array of monoaminergic receptors.

Temporally, changes in [^{11}C]DASB and extracerebral BOLD predominated in the first 30 minutes after the challenge, both reaching over 90% of their respective maximal changes at this time point. Therefore, the two readouts likely reflect the direct molecular and vascular effects of MDMA discussed above. This finding is consistent with previous work indicating peak serotonin release 20 minutes after intraperitoneal MDMA injection [13]. In contrast, increases in [^{18}F]FDG fPET, likely reflecting increased neuronal activity, did not reach a plateau 60 minutes after the challenge at the end of the experiment, suggesting prolonged activation after the peak of direct MDMA action.

Further considerations

Other factors may play a role in the findings. First, MDMA and endogenous serotonin bind to other receptors highly expressed in the brain, such as the 5-HT_1 receptor family [5, 58], which could also be involved in the observed effects. Next, the neuronal activations indicated by fPET could be caused by the effects of MDMA on other neurotransmitters, primarily norepinephrine and dopamine [13, 59]. Dopamine, similarly to serotonin, has been shown to cause vasoconstriction when released at high concentrations [60]. However, the strong correlation between SERT occupancy and hemodynamic changes implies that serotonin is more actively modulating brain microcirculation after acute MDMA application than other monoamines, as previously postulated [9, 14, 33]. To understand how exactly regional hemodynamic and metabolic changes occur, distributions of all drug targets are generally required. PET/MRI imaging offers the opportunity to elucidate the effects of psychedelic drugs by combining data on transporters and receptors with hemodynamics measured by BOLD-fMRI. Recent work has demonstrated how insight into different receptor

distributions can be used to understand changes in BOLD-fMRI data [5]. Such analytical approaches are of interest to gain a deeper understanding of drug mechanisms of action. A more thorough discussion on the advantages and limitations of multimodal imaging and small-animal imaging can be found in *supplementary information*.

5. Conclusion

The present study pioneers and demonstrates the tremendous potential of multimodal imaging in psychedelic drug research. We demonstrate the neurovascular uncoupling induced by an acute MDMA challenge, characterized by increased neuronal activity in monoaminergic projection areas accompanied by vascular depression caused, at least in part, by serotonin release. Our results provide tremendous insight into the mechanism of action of MDMA and pave the way for the application of hybrid PET/fMRI in psychedelic drug research.

Funding

The research was funded by the Eberhard Karls University Tübingen, Faculty of Medicine (fortüne 2209-0-0 and 2409-0-0) to HFW, the Carl Zeiss Foundation to KH and the Werner Siemens Foundation to BJP.

CRediT authorship contribution statement

Tudor M. Ionescu: Conceptualization, Methodology, Software, Validation, Formal analysis, Data curation, Writing – original draft, Visualization. **Mario Amend:** Conceptualization, Methodology, Investigation, Writing – review & editing, Supervision. **Tadashi Watabe:** Methodology, Investigation, Writing – review & editing. **Jun Hatazawa:** Writing – review & editing. **Andreas Maurer:** Writing – review & editing. **Gerald Reischl:** Writing – review & editing. **Bernd J Pichler:** Writing – review & editing, Funding acquisition. **Hans F. Wehrl:** Conceptualization, Methodology, Writing – review & editing, Funding acquisition, Visualization. **Kristina Herfert:** Methodology, Writing – review & editing, Funding acquisition, Visualization.

Declaration of Competing Interests

The authors declare no conflict of interest.

Acknowledgements

We acknowledge Dr. Julia Mannheim, Dr. Rebecca Rock, Dr. Neele Hübner, Dr. Andreas Dieterich, Ines Herbon, Stacy Huang, Sandro Aidone, and Linda Schramm for their administrative and technical support. We thank the Radiopharmacy department for tracer production. This work is also part of the Ph.D. thesis of Tudor M Ionescu.

6. Bibliography

1. Carhart-Harris RL, Goodwin GM. The Therapeutic Potential of Psychedelic Drugs: Past, Present, and Future. Neuropsychopharmacology. 2017;42(11):2105-13. doi: 10.1038/npp.2017.84.
2. Andersen KAA, Carhart-Harris R, Nutt DJ, Erritzoe D. Therapeutic effects of classic serotonergic psychedelics: A systematic review of modern-era clinical studies. Acta psychiatrica Scandinavica. 2021;143(2):101-18. Epub 2020/10/31. doi: 10.1111/acps.13249. PubMed PMID: 33125716.
3. Mitchell JM, Bogenschutz M, Lilienstein A, Harrison C, Kleiman S, Parker-Guilbert K, et al. MDMA-assisted therapy for severe PTSD: a randomized, double-blind, placebo-controlled phase 3 study. Nature Medicine. 2021;27(6):1025-33. doi: 10.1038/s41591-021-01336-3.
4. Carhart-Harris RL, Murphy K, Leech R, Erritzoe D, Wall MB, Ferguson B, et al. The Effects of Acutely Administered 3,4-Methylenedioxymethamphetamine on Spontaneous Brain Function in Healthy Volunteers Measured with Arterial Spin Labeling and Blood Oxygen Level–Dependent Resting State Functional Connectivity. Biological Psychiatry. 2015;78(8):554-62. doi: https://doi.org/10.1016/j.biopsych.2013.12.015.
5. Dipasquale O, Selvaggi P, Veronese M, Gabay AS, Turkheimer F, Mehta MA. Receptor-Enriched Analysis of functional connectivity by targets (REACT): A novel, multimodal analytical approach informed by PET to study the pharmacodynamic response of the brain under MDMA. NeuroImage. 2019;195:252-60. Epub 04/04. doi: 10.1016/j.neuroimage.2019.04.007. PubMed PMID: 30953835.
6. Carhart-Harris RL, Erritzoe D, Williams T, Stone JM, Reed LJ, Colasanti A, et al. Neural correlates of the psychedelic state as determined by fMRI studies with psilocybin. Proceedings of the National Academy of Sciences. 2012;109(6):2138-43. doi: 10.1073/pnas.1119598109.
7. Barrett FS, Krimmel SR, Griffiths RR, Seminowicz DA, Mathur BN. Psilocybin acutely alters the functional connectivity of the claustrum with brain networks that support perception, memory, and attention. NeuroImage. 2020;218:116980. doi: https://doi.org/10.1016/j.neuroimage.2020.116980.
8. Gabay AS, Kempton MJ, Gilleen J, Mehta MA. MDMA Increases Cooperation and Recruitment of Social Brain Areas When Playing Trustworthy Players in an Iterated Prisoner's Dilemma. The Journal of Neuroscience. 2019;39(2):307-20. doi: 10.1523/jneurosci.1276-18.2018.
9. Quate L, McBean DE, Ritchie IM, Olverman HJ, Kelly PAT. Acute methylenedioxymethamphetamine administration: effects on local cerebral blood flow and glucose utilisation in the dark agouti rat. Psychopharmacology. 2004;173(3):287-95. doi: 10.1007/s00213-004-1784-z.

554 10. Soto-Montenegro ML, Vaquero JJ, Arango C, Ricaurte G, García-Barreno P,
555 Desco M. Effects of MDMA on blood glucose levels and brain glucose metabolism.
556 European Journal of Nuclear Medicine and Molecular Imaging. 2007;34(6):916-25.
557 doi: 10.1007/s00259-006-0262-8.
558 11. Wilkerson G, London ED. Effects of methylenedioxymethamphetamine on
559 local cerebral glucose utilization in the rat. Neuropharmacology. 1989;28(10):1129-
560 38. doi: https://doi.org/10.1016/0028-3908(89)90128-7.
561 12. Vollenweider FX, Leenders KL, Scharfetter C, Maguire P, Stadelmann O,
562 Angst J. Positron emission tomography and fluorodeoxyglucose studies of metabolic
563 hyperfrontality and psychopathology in the psilocybin model of psychosis.
564 Neuropsychopharmacology. 1997;16(5):357-72. Epub 1997/05/01. doi:
565 10.1016/s0893-133x(96)00246-1. PubMed PMID: 9109107.
566 13. Gough B, Ali SF, Slikker W, Holson RR. Acute effects of 3,4-
567 methylenedioxymethamphetamine (MDMA) on monoamines in rat caudate.
568 Pharmacology Biochemistry and Behavior. 1991;39(3):619-23. doi:
569 https://doi.org/10.1016/0091-3057(91)90137-Q.
570 14. Cohen ZVI, Bonvento G, Lacombe P, Hamel E. SEROTONIN IN THE
571 REGULATION OF BRAIN MICROCIRCULATION. Progress in Neurobiology.
572 1996;50(4):335-62. doi: https://doi.org/10.1016/S0301-0082(96)00033-0.
573 15. Kim JG, Leem Y-E, Kwon I, Kang J-S, Bae YM, Cho H. Estrogen modulates
574 serotonin effects on vasoconstriction through Src inhibition. Experimental & Molecular
575 Medicine. 2018;50(12):1-9. doi: 10.1038/s12276-018-0193-z.
576 16. Van Nueten JM, Janssens WJ, Vanhoutte PM. Serotonin and vascular
577 reactivity. Pharmacological research communications. 1985;17(7):585-608. Epub
578 1985/07/01. doi: 10.1016/0031-6989(85)90067-0. PubMed PMID: 2931729.
579 17. Wehrl HF, Hossain M, Lankes K, Liu CC, Bezrukov I, Martirosian P, et al.
580 Simultaneous PET-MRI reveals brain function in activated and resting state on
581 metabolic, hemodynamic and multiple temporal scales. Nat Med. 2013;19(9):1184-9.
582 doi: 10.1038/nm.3290. PubMed PMID: 23975025.
583 18. Judenhofer MS, Wehrl HF, Newport DF, Catana C, Siegel SB, Becker M, et al.
584 Simultaneous PET-MRI: a new approach for functional and morphological imaging.
585 Nat Med. 2008;14(4):459-65. doi: 10.1038/nm1700. PubMed PMID: 18376410.
586 19. Jonckers E, Shah D, Hamaide J, Verhoye M, Van der Linden A. The power of
587 using functional fMRI on small rodents to study brain pharmacology and disease.
588 Frontiers in Pharmacology. 2015;6(231). doi: 10.3389/fphar.2015.00231.
589 20. Sander CY, Hooker JM, Catana C, Normandin MD, Alpert NM, Knudsen GM,
590 et al. Neurovascular coupling to D2/D3 dopamine receptor occupancy using
591 simultaneous PET/functional MRI. Proceedings of the National Academy of Sciences
592 of the United States of America. 2013;110(27):11169-74. Epub 05/30. doi:
593 10.1073/pnas.1220512110. PubMed PMID: 23723346.
594 21. Hansen HD, Mandeville JB, Sander CY, Hooker JM, Catana C, Rosen BR, et
595 al. Functional Characterization of 5-HT(1B) Receptor Drugs in Nonhuman Primates
596 Using Simultaneous PET-MR. J Neurosci. 2017;37(44):10671-8. Epub 2017/10/04.
597 doi: 10.1523/jneurosci.1971-17.2017. PubMed PMID: 28972127; PubMed Central
598 PMCID: PMCPMC5666586.
599 22. Villien M, Wey H-Y, Mandeville JB, Catana C, Polimeni JR, Sander CY, et al.
600 Dynamic functional imaging of brain glucose utilization using fPET-FDG.
601 NeuroImage. 2014;100:192-9. doi: https://doi.org/10.1016/j.neuroimage.2014.06.025.
602 23. Rischka L, Gryglewski G, Pfaff S, Vanicek T, Hienert M, Klobl M, et al.
603 Reduced task durations in functional PET imaging with [(18)F]FDG approaching that

of functional MRI. Neuroimage. 2018;181:323-30. Epub 2018/07/04. doi: 10.1016/j.neuroimage.2018.06.079. PubMed PMID: 29966719.

24. Morefield KM, Keane M, Felgate P, White JM, Irvine RJ. Pill content, dose and resulting plasma concentrations of 3,4-methylendioxymethamphetamine (MDMA) in recreational 'ecstasy' users. Addiction. 2011;106(7):1293-300. doi: https://doi.org/10.1111/j.1360-0443.2011.03399.x.

25. Reimold M, Smolka MN, Schumann G, Zimmer A, Wrase J, Mann K, et al. Midbrain serotonin transporter binding potential measured with [11C]DASB is affected by serotonin transporter genotype. Journal of neural transmission (Vienna, Austria : 1996). 2007;114(5):635-9. Epub 2007/01/18. doi: 10.1007/s00702-006-0609-0. PubMed PMID: 17225932.

26. Amend M, Ionescu TM, Di X, Pichler BJ, Biswal BB, Wehrl HF. Functional resting-state brain connectivity is accompanied by dynamic correlations of application-dependent [(18)F]FDG PET-tracer fluctuations. Neuroimage. 2019;196:161-72. Epub 2019/04/15. doi: 10.1016/j.neuroimage.2019.04.034. PubMed PMID: 30981858.

27. Matthew Brett J-LA, Romain Valabregue, Jean-Baptiste Poline. Region of interest analysis using an SPM toolbox. 8th Internation Conference on Functional Mapping of the Human Brain. Sendai, JapanJune 2-6, 2002.

28. Schiffer WK, Mirrione MM, Biegon A, Alexoff DL, Patel V, Dewey SL. Serial microPET measures of the metabolic reaction to a microdialysis probe implant. J Neurosci Methods. 2006;155(2):272-84. Epub 2006/03/08. doi: 10.1016/j.jneumeth.2006.01.027. PubMed PMID: 16519945.

29. López-González FJ, Silva-Rodríguez J, Paredes-Pacheco J, Niñerola-Baizán A, Efthimiou N, Martín-Martín C, et al. Intensity normalization methods in brain FDG-PET quantification. NeuroImage. 2020;222:117229. doi: https://doi.org/10.1016/j.neuroimage.2020.117229.

30. Walker M, Ehrlichmann W, Stahlschmidt A, Pichler BJ, Fischer K. In Vivo Evaluation of 11C-DASB for Quantitative SERT Imaging in Rats and Mice. J Nucl Med. 2016;57(1):115-21. Epub 2015/10/31. doi: 10.2967/jnumed.115.163683. PubMed PMID: 26514178.

31. Hodkinson DJ, de Groote C, McKie S, Deakin JFW, Williams SR. Differential Effects of Anaesthesia on the phMRI Response to Acute Ketamine Challenge. Br J Med Med Res. 2012;2(3):373-85. doi: 10.9734/bjmmr/2012/1412. PubMed PMID: 22737655.

32. McKie S, Del-Ben C, Elliott R, Williams S, del Vai N, Anderson I, et al. Neuronal effects of acute citalopram detected by pharmacoMRI. Psychopharmacology (Berl). 2005;180(4):680-6. Epub 2005/05/13. doi: 10.1007/s00213-005-2270-y. PubMed PMID: 15889241.

33. Ferrington L, Kirilly E, McBean DE, Olverman HJ, Bagdy G, Kelly PAT. Persistent cerebrovascular effects of MDMA and acute responses to the drug. European Journal of Neuroscience. 2006;24(2):509-19. doi: https://doi.org/10.1111/j.1460-9568.2006.04923.x.

34. Andrade R. Serotonergic regulation of neuronal excitability in the prefrontal cortex. Neuropharmacology. 2011;61(3):382-6. doi: https://doi.org/10.1016/j.neuropharm.2011.01.015.

35. Shen R-Y, Andrade R. 5-Hydroxytryptamine$_2$ Receptor Facilitates GABAergic Neurotransmission in Rat Hippocampus. Journal of Pharmacology and Experimental Therapeutics. 1998;285(2):805-12.

36. Roseman L, Leech R, Feilding A, Nutt DJ, Carhart-Harris RL. The effects of psilocybin and MDMA on between-network resting state functional connectivity in

655 healthy volunteers. Frontiers in human neuroscience. 2014;8:204-. doi:
656 10.3389/fnhum.2014.00204. PubMed PMID: 24904346.
657 37. Gouzoulis-Mayfrank E, Schreckenberger M, Sabri O, Arning C, Thelen B,
658 Spitzer M, et al. Neurometabolic Effects of Psilocybin, 3,4-
659 Methylenedioxyethylamphetamine (MDE) and d-Methamphetamine in Healthy
660 Volunteers A Double-Blind, Placebo-Controlled PET Study with [18F]FDG.
661 Neuropsychopharmacology. 1999;20(6):565-81. doi: 10.1016/S0893-133X(98)00089-
662 X.
663 38. Ullmer C, Schmuck K, Kalkman HO, Lübbert H. Expression of serotonin
664 receptor mRNAs in blood vessels. FEBS Letters. 1995;370(3):215-21. doi:
665 https://doi.org/10.1016/0014-5793(95)00828-W.
666 39. Gamoh S, Hisa H, Yamamoto R. 5-Hydroxytryptamine Receptors as Targets
667 for Drug Therapies of Vascular-Related Diseases. Biological and Pharmaceutical
668 Bulletin. 2013;36(9):1410-5. doi: 10.1248/bpb.b13-00317.
669 40. Yakovlev DS, Spasov AA, Mal'tsev DV, Anisimova VA. Effect of 5-HT(2A)
670 receptor antagonists on blood flow in the carotid vessels upon elevation of serotonin
671 level. Bulletin of experimental biology and medicine. 2014;157(3):350-2. Epub
672 2014/07/30. doi: 10.1007/s10517-014-2563-4. PubMed PMID: 25070162.
673 41. !!! INVALID CITATION !!! {}.
674 42. Madsen MK, Fisher PM, Burmester D, Dyssegaard A, Stenbæk DS,
675 Kristiansen S, et al. Psychedelic effects of psilocybin correlate with serotonin 2A
676 receptor occupancy and plasma psilocin levels. Neuropsychopharmacology.
677 2019;44(7):1328-34. Epub 01/26. doi: 10.1038/s41386-019-0324-9. PubMed PMID:
678 30685771.
679 43. Passie T, Seifert J, Schneider U, Emrich HM. The pharmacology of psilocybin.
680 Addiction Biology. 2002;7(4):357-64. doi:
681 https://doi.org/10.1080/1355621021000005937.
682 44. Nutt DJ, de Wit H. Putting the MD back into MDMA. Nature Medicine.
683 2021;27(6):950-1. doi: 10.1038/s41591-021-01385-8.
684 45. Sarris J, Pinzon Rubiano D, Day K, Galvão-Coelho NL, Perkins D.
685 Psychedelic medicines for mood disorders: current evidence and clinical
686 considerations. Current Opinion in Psychiatry. 2022;35(1):22-9. doi:
687 10.1097/yco.0000000000000759. PubMed PMID: 00001504-202201000-00005.
688 46. Carhart-Harris RL, Nutt DJ. Serotonin and brain function: a tale of two
689 receptors. Journal of Psychopharmacology. 2017;31(9):1091-120. doi:
690 10.1177/0269881117725915.
691 47. Nutt D, Carhart-Harris R. The Current Status of Psychedelics in Psychiatry.
692 JAMA psychiatry. 2021;78(2):121-2. Epub 2020/07/30. doi:
693 10.1001/jamapsychiatry.2020.2171. PubMed PMID: 32725172.
694 48. Riedl V, Utz L, Castrillón G, Grimmer T, Rauschecker JP, Ploner M, et al.
695 Metabolic connectivity mapping reveals effective connectivity in the resting human
696 brain. Proceedings of the National Academy of Sciences of the United States of
697 America. 2016;113(2):428-33. Epub 12/28. doi: 10.1073/pnas.1513752113. PubMed
698 PMID: 26712010.
699 49. Attwell D, Laughlin SB. An energy budget for signaling in the grey matter of
700 the brain. Journal of cerebral blood flow and metabolism : official journal of the
701 International Society of Cerebral Blood Flow and Metabolism. 2001;21(10):1133-45.
702 Epub 2001/10/13. doi: 10.1097/00004647-200110000-00001. PubMed PMID:
703 11598490.
704 50. Seeley WW, Menon V, Schatzberg AF, Keller J, Glover GH, Kenna H, et al.
705 Dissociable intrinsic connectivity networks for salience processing and executive

706 control. J Neurosci. 2007;27(9):2349-56. Epub 2007/03/03. doi:
707 10.1523/jneurosci.5587-06.2007. PubMed PMID: 17329432; PubMed Central
708 PMCID: PMCPMC2680293.
709 51. Olsen CM. Natural rewards, neuroplasticity, and non-drug addictions.
710 Neuropharmacology. 2011;61(7):1109-22. Epub 04/01. doi:
711 10.1016/j.neuropharm.2011.03.010. PubMed PMID: 21459101.
712 52. Phan KL, Wager T, Taylor SF, Liberzon I. Functional Neuroanatomy of
713 Emotion: A Meta-Analysis of Emotion Activation Studies in PET and fMRI.
714 NeuroImage. 2002;16(2):331-48. doi: https://doi.org/10.1006/nimg.2002.1087.
715 53. Sumnall HR, Cole JC, Jerome L. The varieties of ecstatic experience: an
716 exploration of the subjective experiences of ecstasy. Journal of psychopharmacology
717 (Oxford, England). 2006;20(5):670-82. Epub 2006/01/13. doi:
718 10.1177/0269881106060764. PubMed PMID: 16401654.
719 54. Pfaus JG, Tse TL, Werk CM, Chanda ML, Leblonde A, Harbour VL, et al.
720 Enhanced synaptic responses in the piriform cortex associated with sexual
721 stimulation in the male rat. Neuroscience. 2009;164(4):1422-30. Epub 2009/09/30.
722 doi: 10.1016/j.neuroscience.2009.09.060. PubMed PMID: 19786078.
723 55. Andrade R, Weber E. Htr2a Gene and 5-HT2A Receptor Expression in the
724 Cerebral Cortex Studied Using Genetically Modified Mice. Front Neurosci.
725 2010;4(36). doi: 10.3389/fnins.2010.00036.
726 56. Amargós-Bosch M, Bortolozzi A, Puig MV, Serrats J, Adell A, Celada P, et al.
727 Co-expression and In Vivo Interaction of Serotonin1A and Serotonin2A Receptors in
728 Pyramidal Neurons of Prefrontal Cortex. Cerebral Cortex. 2004;14(3):281-99. doi:
729 10.1093/cercor/bhg128.
730 57. Puig MV, Gulledge AT. Serotonin and prefrontal cortex function: neurons,
731 networks, and circuits. Mol Neurobiol. 2011;44(3):449-64. Epub 11/11. doi:
732 10.1007/s12035-011-8214-0. PubMed PMID: 22076606.
733 58. Paterson LM, Kornum BR, Nutt DJ, Pike VW, Knudsen GM. 5-HT radioligands
734 for human brain imaging with PET and SPECT. Medicinal Research Reviews.
735 2013;33(1):54-111. doi: https://doi.org/10.1002/med.20245.
736 59. Lettfuss NY, Fischer K, Sossi V, Pichler BJ, von Ameln-Mayerhofer A. Imaging
737 DA release in a rat model of L-DOPA-induced dyskinesias: a longitudinal in vivo PET
738 investigation of the antidyskinetic effect of MDMA. Neuroimage. 2012;63(1):423-33.
739 Epub 2012/07/07. doi: 10.1016/j.neuroimage.2012.06.051. PubMed PMID:
740 22766162.
741 60. Brodde OE. Vascular dopamine receptors: Demonstration and
742 characterization by in vitro studies. Life Sci. 1982;31(4):289-306. Epub 1982/07/26.
743 doi: 10.1016/0024-3205(82)90406-4. PubMed PMID: 6292644.

744

745